Suspension platform interferometer for the AEI 10 m prototype: concept, design and optical layout

K Dahl[1], O Kranz[1], G Heinzel[1], B Willke[1], K A Strain[1,2], S Goßler[1] and K Danzmann[1]

[1] Max-Planck-Institut für Gravitationsphysik (Albert-Einstein-Institut) and Institut für Gravitationsphysik, Leibniz Universität Hannover, 30167 Hannover, Germany
[2] SUPA School of Physics & Astronomy, University of Glasgow, Glasgow, G12 8QQ, United Kingdom

E-mail: `katrin.dahl@aei.mpg.de`

Abstract.
  At present a 10 m prototype interferometer facility is being set up at the AEI Hannover. One unique feature of the prototype will be the suspension platform interferometer (SPI). The purpose of the SPI is to monitor and stabilise the relative motion between three seismically isolated optical tables. The in-vacuum tables are suspended in an L-shaped configuration with an arm length of 11.65 m. The design goal of the SPI is to stabilise longitudinal differential displacements to a level of $100 \, \mathrm{pm}/\sqrt{\mathrm{Hz}}$ between 10 mHz and 100 Hz and relative angular noise of $10 \, \mathrm{nrad}/\sqrt{\mathrm{Hz}}$ in the same frequency band. This paper covers the design aspects of the SPI, e.g. cross-coupling between the different degrees of freedom and fibre pointing noise are investigated. A simulation is presented which shows that with the chosen optical design of the SPI all degrees of table motion can be sensed in a fully decoupled way. Furthermore, a proof of principle test of the SPI sensing scheme is shown.

1. Introduction

The AEI 10 m prototype interferometer [1] aims not only at testing and developing new techniques for future upgrades of gravitational-wave detectors, it is also a testbed for ultra-low displacement noise experiments such as to measure the standard quantum limit of interferometry or performing tests for the GRACE follow-on experiment [2]. The prototype has an L-shaped vacuum envelope with an arm length of about 10 m. At each end and in the corner of the 'L' a tank is located, housing a 1.75 m × 1.75 m optical table supported by a seismic attenuation system derived from the HAM-SAS table [3]. Although these tables have been designed to provide excellent seismic isolation, there will still be a certain amount of residual motion between the three tables. The task of the suspension platform interferometer (SPI) is to sense this relative motion and

to allow suppression by actuators which are part of the seismic attenuation system of each optical table.

One of the planned experiments is to perform tests for a GRACE follow-on mission. GRACE [4] consists of two satellites, its goal is to map the Earth's gravity field. The orbital motion of each satellite senses local variations of the Earth's gravity field. This leads to small fluctuations of the inter-satellite distance. In order to test laser interferometers for GRACE follow-on missions, it is planned to perform experiments within the AEI 10 m prototype where the suspended tables represent satellites. By using signals of the SPI, the tables will be moved on purpose by a well-known amount. This experiment sets the design goal for the SPI in the lower frequency range, which is less than $100\,\mathrm{pm}/\sqrt{\mathrm{Hz}}$ between 10 mHz and 100 Hz for longitudinal table motion and $10\,\mathrm{nrad}/\sqrt{\mathrm{Hz}}$ for angular noise in the same frequency band.

The main experiment that will be set up on the tables of the AEI 10 m prototype facility is a Michelson interferometer with Fabry-Perot arm cavities. The scope of this interferometer is to probe at and beyond the standard quantum limit of interferometry [5]. Therefore, all classical noise sources, e.g. seismic noise, have to be sufficiently reduced to leave the sensitivity exclusively limited by quantum noise in the measurement band of interest. A straightforward way to reduce seismic noise is to suspend all optics of the interferometer. The SPI and the table position control act to reduce the relative motion of the tables, and hence stabilises the suspension positions of the suspended interferometer components that are supported by the tables. This stabilisation decreases the required force and hence the noise of the voice coil actuators that are an integral part of the position control of each suspension. The reduced relative velocity of the components also makes it easier for the interferometer control system to acquire lock.

2. Introduction to suspension platform interferometry

The idea to set up an ancillary interferometer beside the main interferometer to improve lock acquisition and the operation of the main interferometer, especially at low frequencies, was proposed by Drever [6]. He suggested to install and lock an ancillary interferometer at the intermediate stage of the suspended mirrors of the main interferometer to reduce their residual rms motions. This idea was tested by Aso et al [7]. They measured 40 dB noise reduction between 0.1 Hz and 1 Hz. In an experiment conducted by Numata and Camp [8], the relative longitudinal and yaw motions between two hexapods separated by 1 m were measured by use of three homodyne Michelson interferometers. The longitudinal displacement was stabilised to $1\,\mathrm{nm}/\sqrt{\mathrm{Hz}}$ at 1 mHz.

The SPI described in this paper is unique in the sense that

- the SPI will monitor the relative motion between three suspended optical tables (weight of about 1 t each and separated by about 10 m).
- the SPI will provide continuous error signals over a wide ($\gg\lambda$) operating range to track the relative table motions.
- the SPI will sense all degrees of freedom except for roll around the beam axis.

Several optical configurations can be used to sense relative motions between two objects, e.g. a Fabry-Perot cavity or an optical configuration using a pseudo-random noise code [9, 10]. The advantage of a Fabry-Perot cavity is that it is a fairly simple setup. The main disadvantage and the reason why it was not an option for the SPI

is the limited sensing range of one cavity linewidth. We decided to use heterodyne Mach-Zehnder interferometry to monitor the relative motions of the three suspended tables. This provides the desired constant sensing performance at any table position over many optical wavelengths. Furthermore, we are able to benefit from in-house experience gained with the experiments for LISA Pathfinder [11].

The optical layout of the SPI is shown in figure 1. It is the result of simulation work taking into consideration several requirements. In this paper the layout is presented first, followed by details of the simulation from which it resulted.

The following nomenclature is used in this paper: all photodiodes are abbreviated with PD followed by another letter that indicates to which interferometer the photodiode belongs (D for diagnostic, R for reference, S for south, and W for west). All beam splitters are abbreviated with BS, all beam recombiners with BR, and all mirrors with M. All optics are placed on the central table except for mirror MS which is placed on the south table and mirror MW which is placed on the west table. The reference beam "beamR" is confined to the baseplate on the central table, while parts of the measurement beam "beamM" also travel to the south and west tables.

3. Optical layout

The SPI consists in total of four non-polarising heterodyne Mach-Zehnder interferometers. All interferometers share the same optical path on the modulation bench, which is shown in the lower left box of figure 1. Here, the laser beam is prepared and coupled into optical fibres. The fibre outcouplers are mounted on the measurement bench located on the central table inside the vacuum system. In contrast to the modulation bench which uses conventional optical mounts, the measurement bench is quasi-monolithic and thus much more stable in terms of mechanical and thermal drifts. All displacement measurements are performed on the measurement bench.

3.1. Modulation bench

The modulation bench housing the laser is located outside of the vacuum system. We choose to work with a continuous-wave laser of a wavelength of 1064 nm and aim to reduce the SPI sensing noise due to laser frequency fluctuations to $10 \, \mathrm{pm}/\sqrt{\mathrm{Hz}}$ at 10 mHz, to make sure that laser frequency noise will not limit the SPI sensitivity. Since the arm length mismatch of two of the four Mach-Zehnder interferometers is about 23 m, the laser frequency stability has to be better than $120 \, \mathrm{Hz}/\sqrt{\mathrm{Hz}}$ at 10 mHz. We choose a commercially available iodine-stabilised Nd:YAG laser [12].

The laser light is split into two paths (at beam splitter BS in the lower left box of figure 1). After that, each of the two beams is frequency-shifted by an acousto-optic modulator (AOM) operating near 80 MHz, with a frequency difference between the two channels set to the desired heterodyne frequency, which has been chosen to be around 20 kHz in order to provide a control bandwidth up to 100 Hz. The light (beamR and beamM in figure 1) is coupled into two 20 m long polarisation-maintaining single-mode optical fibres. These are fed into the vacuum system, and beamR and beamM are delivered to fibre couplers mounted on the measurement bench.
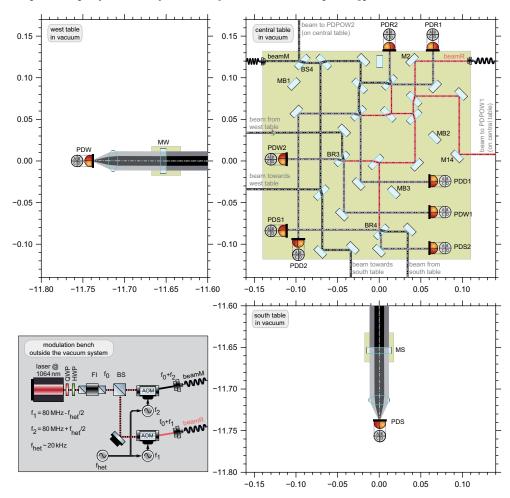
Figure 1: The optical layout of the SPI. The modulation bench which is placed outside the vacuum system is depicted in the lower left. On the modulation bench the laser light is prepared and coupled into optical fibres. These fibres deliver the beams to the measurement bench which is placed on the central table in the vacuum system (see upper right box). The reference beam, beamR, is drawn in red; the measurement beam, beamM, in black. All scales show the distance from the centre of the central table in meter. x = 0 m, y = 0 m is the centre of the central table; x = -11.65 m, y = 0 m is the centre of the west table (upper left box), and x = 0 m, y = -11.65 m is the centre of the south table (lower right box).

3.2. Measurement bench

The measurement bench is located on the central table (inside the vacuum system) and holds the mechanically and thermally ultra-stable part of the four interferometers. To ensure that thermal drifts are kept sufficiently small, the measurement bench is made of Clearceram®-Z HS, an ultra-low expansion material with a coefficient of thermal expansion of $(0.0\pm0.2)\cdot10^{-7}\,\mathrm{K}^{-1}$ and a zero-crossing at room temperature [13]. All beam splitters and mirrors except MS and MW are hydroxy-catalysis bonded [14] to
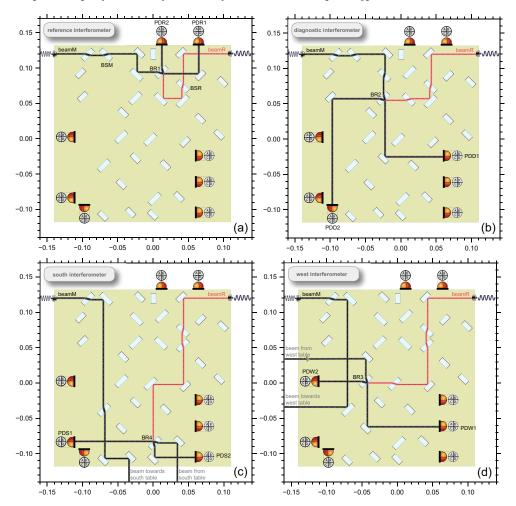
Figure 2: Each of the figures shows the optical path of one of the four interferometers on the measurement bench.

the 250 mm×250 mm surface of the 30 mm thick measurement bench. The remote mirrors MS and MW are bonded on two small cuboids of Clearceram®-Z HS of 35 mm×35 mm and 30 mm height. MS is placed on the south table, MW is placed on the west table.

Except for MS and MW, all mirrors and beam splitters are flat. In order to achieve a high interferometric contrast and a good sensitivity of the differential wave-front sensing signal (DWS) (for further information on DWS see section 4), the radius of curvature of MS and MW has been chosen such that the waist of the two beams is at the recombining beam splitters (BR1, BR2, BR3, BR4). Thus, the beam radius and curvature of the beam's wave front is the same for both interfering beams. This leads to a high interferometric contrast. MS and MW have a radius of curvature of -11.8 m, i.e. they are concave.

One of the four interferometers is the reference interferometer (see figure 2(a)). It is used to cancel common mode fluctuations by subtracting them from all other

interferometer outputs. The reference interferometer measures all path length equivalent fluctuations that have been picked up between the first beam splitter BS on the modulation bench and the recombing beam splitter BR1 on the measurement bench. Therefore, beamR and beamM are recombined at BR1 and their beat note is detected at photodiodes PDR1 and PDR2. Since all interferometers share the same optical paths between the modulation bench and beam splitter BSM and BSR on the measurement bench, all interferometers are affected by the same phase noise. Path length equivalent fluctuations are caused by, e.g. drifts of the conventional mirror mounts on the modulation bench and by stress on and movements of the optical fibres. The optical fibres are flexible but need to be installed loosely so that they do not compromise the excellent seismic isolation of the optical tables.

The second interferometer, the diagnostic interferometer, is also entirely confined to the $250\,\text{mm} \times 250\,\text{mm}$ baseplate (see figure 2(b)). This diagnostic interferometer is the most striking difference of the measurement bench presented in this paper compared to the measurement bench previously shown in [15]. The diagnostic interferometer in conjunction with the reference interferometer will be used for debugging purposes and to determine the sensitivity of the bonded setup since the reference and diagnostic interferomter nominally have the same signals. The diagnostic and reference interferometers are designed such that their optical arm length difference is zero. Within a Mach-Zehnder interferometer of equal arm length, laser frequency noise does not couple into the interferometric output signal. In this way, it is possible to determine the limit to which the south and west tables can be stabilised relative to the central table. A displacement noise measurement between the reference and diagnostic interferometers gives the sensor noise (except laser frequency noise) of the whole SPI. Hence, the limit for stabilising the south and west tables to the central table for an ideal feedback loop. For the diagnostic interferometer the light of beamR and beamM is recombined at BR2 and detected at photodiodes PDD1 and PDD2.

The other two interferometers, namely the west and south interferometers (see figure 2(c)-(d)), measure the displacement and angular deviation of the south/west table relative to the central table. These two interferometers are the so-called measurement interferometers. They are of unequal arm length. One arm of the interferometers (the arm carrying reference beamR) is entirely on the central baseplate. The other arm which is carrying beamM is leaving the central baseplate towards the west table in case of the west interferometer and to the south table in case of the south interferometer. BeamM is reflected back to the measurement bench by MS and MW, respectively.

BeamR and beamM recombine at BR3 and BR4 for the west and south interferometers, respectively. The interference pattern of the west interferometer is detected by photodiodes PDW1 and PDW2, the beat note of the south interferometer at PDS1 and PDS2. A motion of the south/west table can be monitored by the south/west interferometer since the length of the interferometer arm carrying beamM is changing while the south/west table and/or central table is moving, whereas the other arm carrying beamR is of constant length.

The beams reflected by beam splitter BS4 and mirror M14 (see figure 1) are used for power stabilisation and to monitor pointing noise of the fibre injectors. For further details on pointing noise of fibre injectors see subsection 5.2. The light being transmitted by MS and MW due to the residual transmission of the dielectric coating is detected by quadrant photodiodes. These are operated at DC and are used to get additional information of the south and west tables' motion relative to the central

table.

Substrates MB1, MB2, and MB3 (see figure 1) are not part of any of the four interferometers. They are needed as reference within the manufacturing process of the quasi-monolithic measurement bench. The alignment of some of the to-be-bonded mirrors and beam splitters is done either by use of a brass template or by use of a coordinate measurement machine. Between the bonding of the several optics the brass template has to be removed. MB1, MB2, and MB3 define reference points to which the template is realigned when it is placed again onto the measurement bench. For more details on the bonding process and the accuracy achieved see [16].
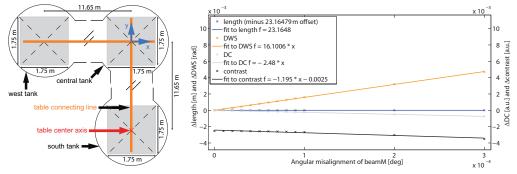
4. Signal processing

The SPI should not only be able to monitor longitudinal relative table motion, but also pitch and yaw motion of the tables. Hence, all photodiodes used for the SPI are quadrant photodiodes. To save as much space as possible for other experiments that will be conducted within the AEI 10 m prototype, the photodiodes are mounted on the Clearceram®-Z HS baseplate. While the photodiodes themselves are inside the vacuum system, the related electronics for signal processing is outside. The signals produced by the recombined beams on photodiodes PDR1, PDR2, PDD1, PDD2, PDS1, PDS2, PDW1, and PDW2 are routed to a phasemeter as developed for LISA Pathfinder experiments [17]. The photocurrents from the other diodes, i.e. PDPOW1, PDPOW2, PDS, and PDW, are routed to signal conditioning electronics.

Each channel of signal conditioning electronics is basically a transimpedance amplifier that converts photo currents into voltages. As well as the voltage for each quadrant, outputs are provided for the sum of all quadrants, the difference between upper and lower quadrants, and the difference between left and right quadrants. All outputs are fed from the signal conditioning electronics into a realtime Control and Data System (CDS) which was developed for the LIGO project [18] and adopted for the AEI 10 m prototype. Within the CDS all signals are digitised and used to monitor and control beam pointing and the tables' relative motion.

The signals from the photodiodes (listed above) which detect recombined beams, are fed to the phasemeter where they are converted to voltages, digitised and Fourier-transformed at the heterodyne frequency by a single-bin discrete Fourier transform. The phasemeter output values for each photodiode quadrant are the DC signal, and the real and imaginary part of the complex amplitude of the photodiode signal at the heterodyne frequency. The argument of the complex amplitude is the phase signal. The phasemeter outputs are transmitted to the CDS via a microcontroller-based phasemeter interface. Within the CDS the signals are combined such that for each quadrant photodiode longitudinal phase information, differential wave-front sensing (DWS) [19] signals for pitch and yaw, differences of left and right as well as bottom and top of the DC photodiode signals, and the interferometric contrast are available. These signals are used to derive error signals for feedback control of the optical tables via voice-coil actuators as described below.

5. Simulation work for the design of the optical layout

Within the process of designing, we minimised coupling of table rotation to the translational motion and investigated the coupling factors. Further simulations were carried out to determine whether the beam pointing noise of the fibre injectors might

(a) Explanation of table central axis   (b) Coupling of pointing noise of beamM to the output signals.
and connecting line.

Figure 3: (a) This sketch explains what is meant by table central axis and connecting
line. The coordinate system used throughout all simulations is given in blue. (b) This
graph shows simulation results how pathlength, DWS, DC, and contrast change in
dependence of angular misalignment of the fiber injector of beamM. The signals of
photodiodes PDS1 and PDR2 have been subtracted and a fit to the data has been
done.

spoil the SPI signals. All simulations including the design of the optical layout have
been done with Optocad [20] and partly with Ifocad.

Due to the symmetric table design the table rotates around its central axis. Thus,
coupling of table rotation to the translational motion is minimised if the far mirrors
MS and MW (see figure 1) are placed in the centre of the south and west tables,
respectively, and the recombining beam splitters BR3 and BR4 are placed along the
table centre connecting line (see figure 3a).

To make the control of the west and south interferometers as close to identical as
possible, both the west and south interferometers, have a design value of arm length
mismatch of 23165 mm. The arm length mismatch of the reference and diagnostic
interferometers is designed to be identical, too. The nominal arm length mismatch of
the interferometers is in reality limited by the accuracy of the assembly process of the
measurement bench, i.e. in the order of a few μm.

5.1. Coupling factors

To check how well the different relative table motions are decoupled we calculated
the coupling factors for the west and south interferometers. A coupling factor is the
first derivative of a signal by a degree of freedom (DoF). A set of coupling factors
calculated for photodiode PDS2 of the south interferometer is shown in table 1.

To obtain the coupling factors shown in this table, mirror MS was moved in 50
steps $\pm 100\,\mu$m or $\pm 4\,\mu$rad away from the well-aligned configuration. This movement of
MS, which is in reality a motion of the south table, was performed in two translational
degrees of freedom and in the yaw degree of freedom since Optocad can cope with
two dimensions only. At each single position of MS pathlength, DWS, DC, and
interferometric contrast of PDS2 were calculated. The coupling factors were then
found by taking the ratios of all of the output signals to each of the input motions.

Table 1: Coupling factors between motion in the table degree of freedoms and SPI sensing signals. These coupling factors were calculated for simulated motions of mirror MS and detection at photodiode PDS2. A motion of MS in the simulation is equivalent to motion of the south table in the experiment. The values for length, DWS, and DC are slopes with a zero-crossing at the properly aligned configuration for all investigated degrees of freedom.

Signal	Length	DWS	DC
DoF	(m/m)	(rad/m)	(a.u./m)
Transversal	3.5e-09	-3.2e+02	2.3e+03
Longitudinal	2.0e+00	1.8e+00	-8.9e-02
	(m/rad)	(rad/rad)	(1/rad)
Rotational	1.2e-07	-3.7e+03	2.8e+04

The length channel is the dedicated channel to monitor relative longitudinal motions of the tables. From the column called 'Length' in table 1 one can clearly see that almost no coupling of the transversal and rotational motion of the south table into the length signal occurs. Thus, it will be possible to distinguish longitudinal relative table motion from any other possible table motion. In the experiment the longitudinal degree of freedom will be the first one to be controlled. A rotation of the south table can be easily monitored by the DWS signal since the factor for DWS rotation is an order of magnitude larger for rotation than for any other possible table motion (see third column in table 1). Rotation will be the second degree of freedom that will be stabilised. The transversal table motion will be monitored by the DC channels. Though the factor is much larger for rotation than for transversal motion, it is still possible to distinguish between the two motions because the rotation of a table was stabilised before by using the DWS signals. Thus, the only remaining motion that can produce a signal in the DC channel is the table's transversal motion.

It will be easily possible to distinguish between rotational and longitudinal relative table motion. Thus, the optical layout as depicted in figure 1 is suitable to achieve the SPI's design goal. During the installation of the SPI the coupling factors will be determined experimentally by moving the table and measuring the table's position by LVDTs (linear variable differential transducer).

5.2. Pointing noise of fibre injectors

A potential noise source is the pointing noise of the fibre injectors. We use a custom-made vacuum compatible version of the adjustable optics holder AAH 5 axes by miCos. They are the only potentially unstable components of the in-vacuum setup since all mirrors and beam splitters are bonded onto an ultra-low expansion baseplate. The idea of having the reference interferometer is to measure all potential instabilities and subtract them from the measurement interferometers, which are the west and south interferometers. In the measurement interferometers the optical path length of beamM is about a factor of 80 longer than in the reference interferometer, i.e. the measurement interferometers are much more sensitive to pointing noise of beamM than the reference interferometer. Thus, pointing noise of a fibre injector could misleadingly

be understood as a relative table motion.

In the simulation beamR was fixed and beamM was moved in yaw. The signals of the photodiodes of the south, west, and reference interferometers were then evaluated. Figure 3b shows exemplarily for PDS1 and PDR1, that beam pointing noise couples into the DWS signal and cannot be removed by subtracting the signal of the reference interferometer from the signals of the south interferometer. To substract the signals of the south interferometer from the signals of the west interferometer is not an option since then no monitoring of the relative table motion would be possible anymore.

The design goal for angular noise in the SPI sensing is $10\,\mathrm{nrad}/\sqrt{\mathrm{Hz}}$ from $10\,\mathrm{mHz}$ up to $100\,\mathrm{Hz}$. To check up to which value of fibre injector pointing noise this can be achieved, a linear fit to the DWS output values as depicted in figure 3b was performed. According to the fit to the DWS signal the beam pointing noise has to be below $11\,\mathrm{prad}/\sqrt{\mathrm{Hz}}$ to reach the design goal for angular noise.

Thus, the pointing noise of the fibre injectors will be monitored by additional non-coherent quadrant photodiodes PDPOW1 and PDPOW2 (see grey labels in upper right box of figure 1) and probably corrected in signal post-processing. The optical pathlength to PDPOW1 and PDPOW2 will be about $70\,\mathrm{cm}$. The pathlength from the beam injector to PDR1 and PDR2 is only about 30 cm. This results in a 7/3 better sensitivity for the DC signal in beam pointing for PDPOW1 and PDPOW2 than for PDR1 and PDR2.

The fit to the phase signal in figure 3b indicates that there is no coupling from pointing noise of beamM into the longitudinal phase channel. However, Guzmán Cervantes et al. [21] have measured that angular noise couples to some extent into the longitudinal phase signal. They further demonstrated that by determining the coupling factors, the angular noise can be well subtracted from the longitudinal phase channel.

If beam pointing limits the sensitivity of the SPI, we will post-process the data and the current fibre injectors will be replaced by monolithic fibre injectors. These injectors were not available at the beginning of the SPI construction. Dedicated space to bond the monolithic fibre injectors on the measurement bench has been left in front of beam splitter BS4 and mirror M2.

6. Test setup

During the design process we have built a test setup to measure the relaitve motion between two standard optical tables. The test setup includes reference and south interferometers as well as an additional Michelson interferometer for calibration. All optics other than mirror MS belonging to the south interferometer were on one optical table. Only MS was on another optical table. The arms of the reference interferometer were of about equal length. The arm length difference of the south interferometer was about $3\,\mathrm{m}$. The radius of curvature of mirror MS was $-2\,\mathrm{m}$. MS was mounted in a piezo-driven mirror mount and placed on two linear stages. In this way, MS could be moved in pitch and yaw as well as longitudinal and transversal relative to the optical table hosting the rest of the south interferometer. A Michelson interferometer was used to calibrate the piezo-driven mirror mount and the linear stages.

Figure 4a shows the signals when MS is moved away from the rest of the interferometer. There is only a change in the longitudinal signal and no coupling into the pitch and yaw channels. If MS is moved in pitch (see figure 4b) the pitch DWS and pitch DC signals clearly indicate a pitch motion. The small coupling into

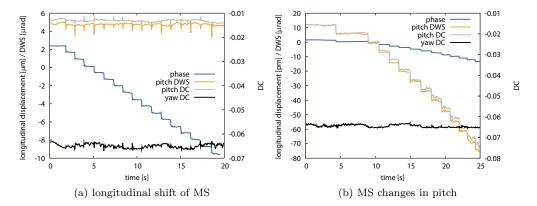(a) longitudinal shift of MS

(b) MS changes in pitch

Figure 4: Signals of the test setup (a) if mirror MS is shifted away from the residual optical setup and (b) if mirror MS is moved in the pitch degree of freedom.

the longitudinal phase channel is due to the fact that the beam was not centred on the curved mirror MS.

The results of the test setup confirmed our approach to use a set of heterodyne Mach-Zehnder interferometers to monitor the relative motion between the 11.65 m apart optical tables within the vacuum system of the AEI 10 m prototype.

7. Status, conclusion and outlook

In this paper, we introduced the measurement concept and optical layout of the SPI for the AEI 10 m prototype. The results of our test setup show that technique of heterodyne Mach-Zehnder interferometry is suitable to monitor relative table motions. Furthermore, simulations regarding the position and sensitivity of the optical layout of SPI were presented. The results show that the design of the optical layout is suitable to achieve the design goal of $100\,\mathrm{pm}/\sqrt{\mathrm{Hz}}$ from $10\,\mathrm{mHz}$ up to $100\,\mathrm{Hz}$ for displacement noise and $10\,\mathrm{nrad}/\sqrt{\mathrm{Hz}}$ in the same frequency band for angular noise.

Currently, three-quarters of the SPI is already bonded. Around winter 2011/2012, the SPI is going to be installed in the vacuum system of the AEI 10 m prototype after the commissioning of the first two optical tables.

References

[1] Goßler S *et al* 2010 *Class. Quantum Grav.* **27** 084023
[2] Dehne M, Guzmán Cervantes F, Sheard B, Heinzel G and Danzmann K 2009 *J. Phys.: Conf. Ser.* **154** 012023
[3] Stochino A *et al* 2009 *Nucl. Instrum. Methods A* **598** 737

[4] Tapley B, Bettadpur S, Watkins M and Reigber C 2004 *Geophys. Res. Lett.* **31** L09607
[5] Caves C M 1980 *Phys. Rev. Lett.* **45** 75–79
[6] Drever R W P 1987 Outline of a proposed design for a first receiver for installation in the long-baseline facilities, of Fabry-Perot type *LIGO Document* **T870001-00-R**
[7] Aso Y, Ando M, Kawabe K, Otsuka S and Tsubono K 2004 *Phys. Lett. A* **327** 1
[8] Numata K and Camp J 2008 *Appl. Opt.* **47** 6832
[9] Shaddock D A 2007 *Opt. Lett.* **32** 3355
[10] de Vine G *et al* 2009 *Opt. Express* **17** 828
[11] McNamara P, Vitale S, Danzmann K and on behalf of the LISA Pathfinder Science Working Team 2008 *Class. Quantum Grav.* **25** 114034
[12] http: //innolight.de/pdf/laser_accessories.pdf
[13] Nakajima K and Nakajima T 2004 *Proc. SPIE* **5567** 1385
[14] Elliffe E J *et al* 2005 *Class. Quantum Grav.* **22** 257
[15] Dahl K *et al* 2010 *J. Phys.: Conf. Ser.* **228** 012027
[16] Dahl K *et al* Bonding accuracy of a suspension platform interferometer with 23 m long arms *in prep*
[17] Heinzel G *et al* 2004 *Class. Quantum Grav.* **21** S581
[18] Shoemaker D 2009 Advanced LIGO Reference Design *LIGO Document* **M060056-v1** https: //dcc.ligo.org/cgi-bin/DocDB/ShowDocument?docid=1507&version=1
[19] Morrison E, Meers B, Robertson D and Ward H 2004 *Appl. Opt.* **33(22)** 5037–5041
[20] Schilling R 2010 OPTOCAD: (0.90c) A Fortran 95 module for tracing Gaussian TEM$_{00}$ beams through an optical set-up *Simulation tool http://www.rzg.mpg.de/∼ros/optocad.html*
[21] Guzmán Cervantes F, Steier F, Wanner G, Heinzel G and Danzmann K 2008 *Appl. Phys. B* **90** 395